PHYSICAL REVIEW B **72**, 075341 (2005)

Interface effect of InSb quantum dots embedded in SiO_2 matrix

Dongliang Chen,[1] Chaosheng Li,[2] Zhengang Zhu,[2] Jiangwei Fan,[1] and Shiqiang Wei[1,*]
[1]*National Synchrotron Radiation Laboratory, University of Science and Technology of China, Hefei, Anhui 230029, People's Republic of China*
[2]*Key Laboratory of Materials Physics, Institute of Solid State Physics, Chinese Academy of Sciences, PO Box 1129, Hefei 230031, People's Republic of China*

(Received 28 December 2004; revised manuscript received 28 June 2005; published 16 August 2005)

The interface effect of InSb quantum dots (QDs) embedded in SiO_2 matrix has been investigated by Raman scattering spectroscopy, x-ray diffraction (XRD), and x-ray absorption fine structure (both of EXAFS and XANES). The EXAFS and XRD results show clearly that the bond length of the Sb-In first shell of the InSb QDs contracts slightly about 0.02 Å compared with that of the bulk InSb. The Raman scattering spectrum of the InSb QDs reveals that the lattice contraction partly weakens the phonon confinement effect. The coordination geometry at the interface of the InSb QDs is mainly Sb (In)-O covalent bridge bonds. The Sb *K*-XANES calculations of InSb QDs embedded in SiO_2 matrix based on FEFF8 indicate that the intensity increase and the broadening of the white line peak of Sb atoms are essentially attributed to both the increase of Sb *p*-hole population and the change of Sb intra-atomic potential $\mu_0(E)$ affected by the SiO_2 matrix. Our results show that the interface effect between the InSb QDs and the SiO_2 matrix leads not only to the slight lattice contraction of InSb QDs and the large structural distortion in the interface area of InSb QDs, but also to the significant change of the Sb intra-atomic potential and the obvious charge redistribution around Sb atoms.

DOI: 10.1103/PhysRevB.72.075341 PACS number(s): 61.46.+w, 79.60.Jv, 61.10.Ht

I. INTRODUCTION

Nanosize materials have attracted considerable attention because their electronic, optical, magnetic, and chemical properties differ dramatically from the respective bulk materials in a size-dependence manner.[1–5] The synthesis of semiconductor quantum dots (QDs) provides very interesting substances due to size-dependence or quantum confinement effect, opening a way to the fabrication of new optoelectronic devices, lasers, and photodetectors.[6–11] Especially, due to the larger exciton Bohr radius and the smaller band gap, the semiconductor InSb QDs have shown fascinating optical properties, such as enhanced nonlinear optical response,[12] large blueshift of optical absorption edge spectral regime from the infrared to the ultraviolet,[13] and photoluminescence (PL) wavelength extended to about 2 μm.[14–16] This reveals some potential applications on fabrication of high-performance optoelectronic devices using the InSb QDs.

There are two important features in the nanometer materials. One is the quantum/phonon confinement effect (i.e., the size effect)[17,18] and the other is the contribution of the surface and the interface effect.[19] In fact, the surface or the interface environment of nanoparticles (NPs) can substantially modify the structures and the properties of NPs. For example, Zhang *et al.* have reported that a reversible structural transformation of semiconductor ZnS QDs with an average size of about 3 nm occurs, driven by water on the surface of ZnS QDs accompanying methanol desorption.[20] This indicates that the binding of water to the surface of ZnS QDs at room temperature leads to a significant structural modification. Daldoss *et al.* have studied the interface region of isolated nanocrystalline Si embedded in SiO_2 matrix by x-ray absorption fine structure (XAFS) and photoluminescence.[21] Their results have shown that the interface region is amorphouslike and plays an active role in the light-emission process. Armelles *et al.*[22] and Zhu *et al.*[23] have reported that the obvious blueshift of Raman peaks have been observed in the InSb QDs capped by InP and in the InAs QDs embedded in SiO_2 matrix. The strong compressive strains of the InSb QDs and the InAs QDs result in lattice contractions of InSb and InAs QDs. Recently, we have investigated the local structure and the electronic distribution of the metallic Co NPs embedded in C_{60} matrix by fluorescence XAFS.[24] It can be found that there are strong interactions between the Co NPs and the C_{60} matrix, and the electrons are transferred from Co atoms to C_{60} molecules. Similarly, Zhang *et al.*[19] have done a systematic study on the local structure and the electronic behavior of alkanethiolate-capped metallic Au NPs with XAFS, x-ray powder diffraction (XRD), and x-ray photoemission spectroscopy (XPS). They have noted that the lattice contraction and the d electron depletion of Au NPs relative to the bulk Au increase with the decrease of NP size. More recently, a direct observation of ferromagnetic spin polarization in Au nanoparticles has been reported by Yamamoto *et al.*[25] for the interaction between the surface of the Au nanoparticles and the polymer. Therefore, the local structures, the electronic behaviors and the optical properties of NPs depend strongly on the interaction between NPs and the capped materials or the embedded matrix. Although the interface effect plays a crucial role in the capped-NP materials and the semiconductor InSb QDs exhibit novel optical properties, little is known about the atomic structures and the interactions between the InSb QDs and the SiO_2 matrix. This is due largely to the difficulty in fluorescence XAFS measurement of InSb and the complexity of the interface structure of NPs. Fortunately, the application of the high-brilliance and high-energy synchrotron radiation light source in SPring-8 with the energy of 8 GeV in storage ring makes it possible for the Sb *K*-edge fluorescence XAFS

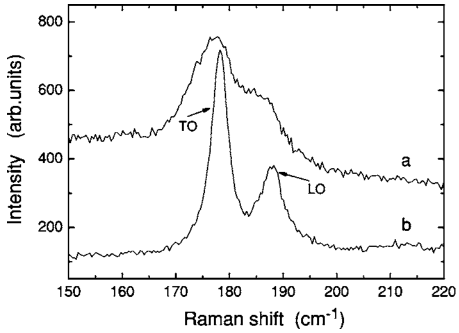

FIG. 1. Raman scattering spectra. (a) As-deposited thin film of InSb QDs. (b) Bulk InSb.

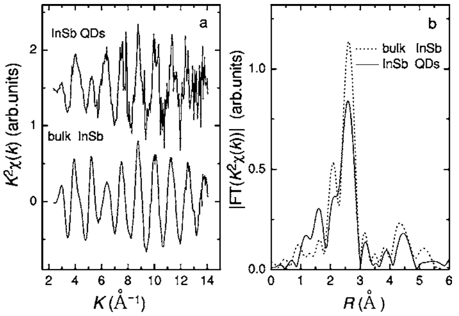

FIG. 2. (a) Sb K-edge EXAFS functions $k^2\chi(k)$ of the bulk InSb and the InSb QDs. (b) Fourier transformations (FTs) of the bulk InSb and the InSb QDs.

measurement using a 19-element high purity Ge solid detector.

In this approach, we combine the Raman scattering (RS) spectroscopy, XRD, and fluorescence XAFS to probe the atomic structures of the InSb QDs and the interaction between the InSb QDs and the SiO_2 matrix. The x-ray absorption near-edge structure (XANES) simulation based on FEFF8 is employed to investigate how SiO_2 matrix affects the Sb K-edge XANES spectrum of the InSb QDs embedded in SiO_2 matrix.[26] We focus mainly on the bridge bonds between the interface of InSb QDs and the SiO_2 matrix, and the changes of the atomic structure and the electronic redistribution caused by the interaction between the InSb QDs and the SiO_2 matrix.

II. EXPERIMENTAL

The thin film of semiconductor InSb QDs embedded in SiO_2 matrix grown on a Si (111) substrate was prepared by magnetron sputtering using codeposition method. The base pressure of the growth chamber was 2.0×10^{-4} Pa. The target was SiO_2 quartz plate of 61mm in diameter on which six small chips of single crystal InSb with a high purity of 99.999% were mounted. The cosputtering was carried out at an Ar pressure of 3.0×10^{-1} Pa. During the codeposition, the temperature of Si substrate was kept at 573 K. The thickness of the thin film for the InSb QDs embedded in SiO_2 matrix was about 1 μm.

The RS spectra of InSb QDs and bulk InSb samples were obtained at room temperature in the backscattering configuration on a LABRAM-HR Raman spectrophotometer using the 514.5 nm line of an Ar^+ laser. The XRD patterns of the InSb QDs and the mixture of polycrystalline InSb and Si powder were recorded on a MXPAHF x-ray diffractometer using Cu K_α x-ray source ($\lambda=0.154056$ nm) in the range of $2\theta=20°–50°$.

The Sb K-edge XAFS spectra of InSb samples were measured at BL01B1 XAFS station of SPring-8 of Japan Synchrotron Radiation Research Institute.[27] The electron energy was 8 GeV with a maximum current of 100 mA. The high brilliance x-ray light source covering a wide energy range (4–110 keV) was coming from the bending magnets. A fixed-exit Si (311) two-flat crystal was used as monochromator. For the higher harmonics rejection an Rh-coated quartz mirror was used. The XAFS data of InSb QDs embedded in SiO_2 matrix grown on Si (111) substrate were collected by fluorescence XAFS with a 19-element high-purity Ge solid detector at room temperature, and the XAFS data of InSb powder were collected in transmission mode using ion chambers filled with the mixed gas of Kr/Ar. XAFS data were analyzed by USTCXAFS3.0 (Ref. 28) and UWXAFS3.0 codes.[29]

III. RESULTS

The RS spectra of the InSb QDs and the bulk InSb are shown in Fig. 1. It can be observed that two Raman peaks corresponding to transverse-optic (TO) and longitudinal-optic (LO) modes appear in the RS spectrum located at 178.3 and 188.0 cm^{-1} for the bulk InSb, respectively. Similarly, there are two Raman peaks located at 177.2 and 185.5 cm^{-1} in the RS spectrum of the InSb QDs. Compared with the bulk InSb, the positions of RS peaks labeled with TO and LO for the InSb QDs shift to lower frequency by 1.1 and 2.5 cm^{-1}, respectively, and the LO peak of the InSb QDs almost disappears. Both the redshift and the asymmetric

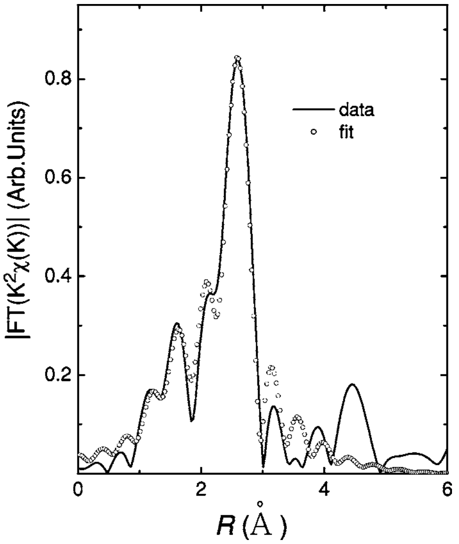

FIG. 3. Fitting curve of Fourier transformations (FTs) for the InSb QDs.

TABLE I. The EXAFS fitting parameters of the bulk InSb and the InSb QDs.

InSb	Band type	N	R	ΔR	$\sigma^2(10^{-3}$ Å)	$C_3(10^{-5}$ Å)	$C_4(10^{-5}$ Å)	ΔE_0(eV)
Bulk	Sb-In	4.0	2.81	−7.51	5.04	3.39	0.174	4.4
QDs	Sb-In	2.8	2.79	−15.4	5.59	3.22	2.35	1.8
	Sb-O	1.0	1.86	−118	3.63	−70.8	146	4.6

broadening towards the low-frequency side have been found for the InSb QDs, showing a strong phonon confinement effect in the InSb QDs embedded in SiO_2 matrix. This is in good agreement with these results reported by Child *et al.*,[16] Shi *et al.*,[30] and Richter *et al.*[31]

The Sb K-edge EXAFS functions $k^2\chi(k)$ and their Fourier transformations (FTs) of the bulk InSb and the InSb QDs are shown in Figs. 2(a) and 2(b), respectively. It can be observed from Fig. 2(a) that the positions of the oscillation peaks of $k^2\chi(k)$ function of the InSb QDs are nearly the same as those of the bulk InSb; whereas the intensities of the oscillation peaks of the InSb QDs are evidently different from those of the bulk InSb in the range of 3.1 to 7.7 $Å^{-1}$. The intensities of the oscillation peaks located at 2.9, 3.9, and 5.3 $Å^{-1}$ for the InSb QDs decrease obviously compared with those of the bulk InSb. Especially, the intensity of the peak located at 5.3 $Å^{-1}$ for the InSb QDs is about 60% weaker than that of the bulk InSb. On the contrary, the intensity of the peak located at 6.4 $Å^{-1}$ for the InSb QDs is about 35% larger than that of the bulk InSb. However, Fig. 2(b) shows that the FT main peak position (R=2.60 Å) of the Sb-In first shell of the InSb QDs is identical with that of the bulk InSb. The shoulder peak at 2.20 Å for both the InSb QDs and the bulk InSb originates from the nonlinearity of the phase shift function of backscattering atom In. The intensity of the main peak of the InSb QDs drops significantly by about 25%, relative to that of bulk InSb. In addition, a small peak corresponding to the Sb-O first shell appears at about 1.60 Å for the InSb QDs.

To obtain the structural parameters of InSb QDs, the least-squares curve fitting was performed for the EXAFS data analysis using the UWXAFS3.0 code.[29] The theoretical amplitude functions and phase shifts were calculated by FEFF8. In order to investigate the moderate disorder and the anharmonicity of the Sb-In pair of the InSb QDs, the cumulant expansion up to the fourth-order terms was employed to fit the EXAFS curve of the InSb QDs in the R range of 0.79 to 3.01 Å using the Sb-In first shell and the Sb-O first shell based on the method reported by Dalba *et al.*[32] and Newville.[33] The anharmonic mean force potential $V(R)$ of the Sb-In first shell can be reconstructed from the first four cumulants. S_0^2 was set at 0.98. The EXAFS fitting results are summarized in Table I and the FT fitting in R space and the anharmonic mean force potential $V(R)$ of the bulk InSb and the InSb QDs are shown in Fig. 3 and 4, respectively.

Seen from Table I, the bond length $R_{\text{Sb-In}}$ and the coordination number N of the Sb-In first shell for the bulk InSb are 2.81 Å and 4.0, respectively. According to the relations between the first four cumulants and the force constants a, b and c of the anharmonic mean force potential $V(R)$,[32,33] one can easily evaluate the anharmonic force constants $a=5.27$ eV/Å^2, $b=-1.30$ eV/Å^3, and $c=1.11$ eV/Å^4. Meanwhile, it can be found that the structural parameters of InSb QDs are significantly different from those of the bulk InSb. The bond length $R_{\text{Sb-In}}$ of the Sb-In first shell of the InSb QDs is 2.79Å, slightly contracted in comparison with that of the bulk InSb. The coordination number $N_{\text{Sb-In}}$ of the Sb-In first shell of the InSb QDs reduces to 2.8. Hence, the anharmonic force constants are $a=4.54$ eV/Å^2, $b=-1.13$ eV/Å^3, and $c=3.68$ eV/Å^4. As shown in Fig. 4, it can be directly observed that for the InSb QDs, the $V(R)$ is evidently asymmetrical and the minimum of $V(R)$ shifts slightly to the left side. Moreover, a strong Sb-O coordination appears in the first shell around the Sb atoms of the InSb QDs, which is due to the surface interaction between the InSb QDs and the SiO_2 matrix. The average bond length $R_{\text{Sb-O}}$ and the coordination number $N_{\text{Sb-O}}$ of the Sb-O first shell are 1.86 Å and 1.0 for the InSb QDs, respectively.

The XRD patterns of the InSb QDs and the bulk InSb are shown in Fig. 5. The bulk InSb is mixed with crystalline Si

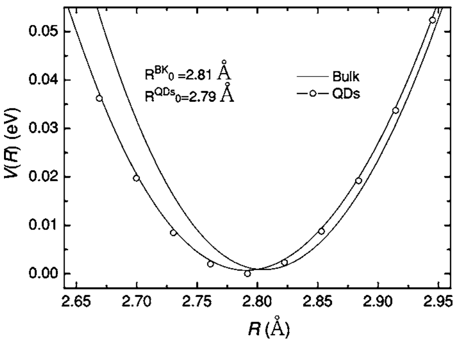

FIG. 4. Anharmonic mean force potential $V(R)$ of the Sb-In first neighbor for the bulk InSb and the InSb QDs.

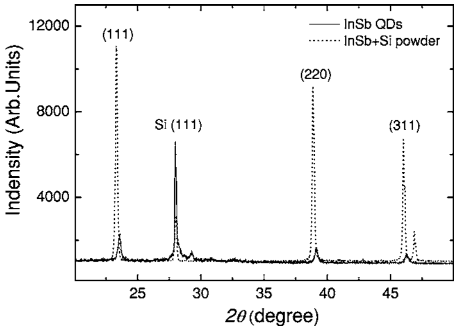

FIG. 5. XRD patterns of as-deposited thin film of InSb QDs (solid line), in which the (111) diffraction peak of silicon is from the Si substrate, and mixture of both InSb and Si powder (dotted line).

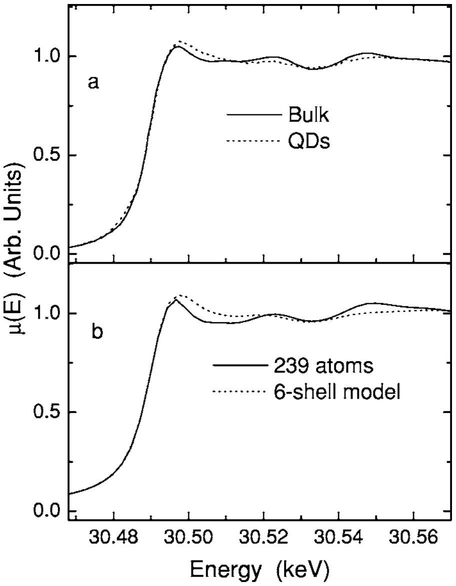

FIG. 6. (a) Sb *K*-XANES experiment spectra of the Bulk InSb and the InSb QDs. (b) Sb *K*-XANES calculated-spectrum of the bulk InSb concluding 239 atoms and the average spectrum of six-shell InSb QDs for the Sb absorber atom at center, second shell, fourth shell and sixth shell of the six-shell InSb cluster.

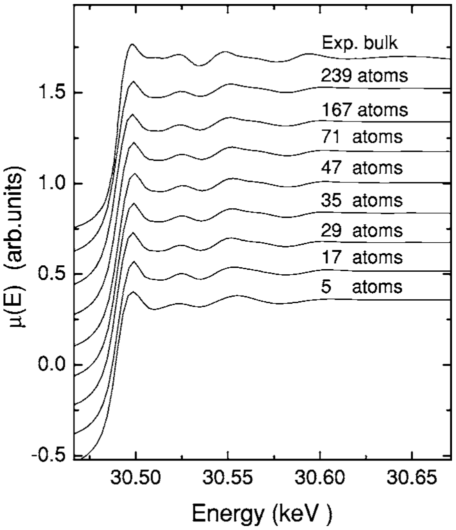

FIG. 7. Sb *K*-XANES calculated-spectrum of the InSb clusters with different coordination shells.

powder to calibrate the diffraction peak positions of the InSb QDs and the bulk InSb. It can be seen that there are obvious shifts up to high 2θ direction in the (111), (220), and (311) diffraction peaks of the InSb QDs. This indicates that the lattice of the InSb QDs (or the InSb nanocrystals) embedded in SiO_2 matrix contracts evidently. The average lattice contraction of the InSb QDs is about 0.51%, relative to that of the bulk InSb. The average size of InSb QDs can be estimated as about 30 nm by Scherrer formula,[34] in which the integral breadths are evaluated after the separation of the α_2 component and corrected for instrumental broadening.

IV. XANES SIMULATION

The Sb *K*-edge experimental XANES spectra of the bulk InSb and the InSb QDs are shown in Fig. 6(a). Compared with those of bulk InSb, the intensity and the width of the "white line" peak of the InSb QDs increases. In order to investigate the XANES spectrum, we have attempted to model a realistic InSb QDs embedded in SiO_2 matrix by placing a InSb cluster into a SiO_2 matrix with the embedding structure in which the interface structure between the InSb QD and the SiO_2 matrix is simply treated and only those Sb-O bridge bonds with the distance larger than 1.86Å are reserved. Seen from Fig. 5, no diffraction peaks of crystalline SiO_2 appear in the XRD pattern of the InSb QDs. It means that the SiO_2 matrix exists in the form of amorphous structure. Hence, for the purpose of simulating the XANES spectrum of the InSb QDs embedded in the amorphous SiO_2 matrix, we modify the coordination geometry of Si and O atoms in SiO_2 matrix as a random Gaussian function distribution using the perfect crystalline structure of SiO_2.[35] The structural parameters of the InSb QDs are based on the EXAFS fitting results in Table I. A cluster size with the diameter of 18.2 Å is used for the XANES calculations. The cluster of InSb QD includes a six-shell InSb cluster (i.e., 43 Sb and 28 In atoms) with a size of 8.0 Å and several neighbor shells of Si and O atoms (i.e., 74 atoms) in SiO_2 matrix. In the FEFF8 code, the Hedin-Lundqvist model of exchange potential with a 1.8 eV shift and no additional broadening is used for calculation. The calculations are carried out using initial ground-state potentials without a core hole. A NOHOLE card is used to further improve the shape of the white line peak. Thermal disorder at room temperature (300 K) is treated with the correlated Debye model for the bulk InSb.

In order to reproduce the entire fine structure of the Sb *K*-edge XANES (*K*-XANES) of the bulk InSb, the size dependence of the Sb *K*-XANES spectrum needs to be investigated in detail. The structural model of InSb cluster in the one-shell calculation is composed of the central Sb atom and the surrounding In tetrahedron. Each subsequent calculation includes the next coordination shell around the central Sb into the cluster. For all these clusters, the cluster radius of the self-consistent field (SCF) calculation was determined as 9.1 Å, only the cluster radius of full multiple-scattering (FMS) increases with the coordination shells gradually. The Sb *K*-XANES spectra with clusters of various neighbor shells are shown in Fig. 7. It can be found that a cluster including at least 5 shells (i.e., 19 Sb and 28 In atoms) must be taken into account for reproducing all fine structures of the Sb *K*-XANES of the bulk InSb. Therefore, it is reasonable that an InSb sphere cluster with 6 shells (i.e., 43 Sb and 28 In atoms) was selected as the model of InSb QDs for a realistic InSb QD embedded in SiO_2 matrix. Four calculations were performed for the absorber Sb atom at the position of the center of InSb sphere cluster, the second shell, the fourth shell, and the sixth shell. The cluster radii of the FMS and SCF calculations were 8.0 and 9.1 Å, respectively. This is adequate to obtain sufficiently accurate scattering potential

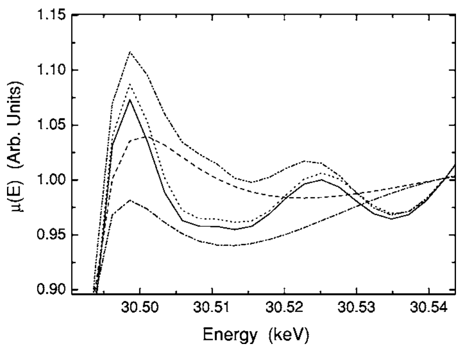

FIG. 8. Effect of the SiO_2 matrix on the InSb cluster. Calculations for a six-shell InSb cluster with (dash–dot-dotted line and dashed line for its μ_0) and without (dotted line and dash-dotted line for its μ_0) SiO_2 matrix, as well as an InSb cluster with 239 atoms for comparison (solid line) normalized at 50 eV above the edge.

of the SiO_2 matrix. Finally, the average of the four Sb *K*-XANES spectra was carried out with the weight of the corresponding numbers of Sb atoms. One can see clearly in Fig. 6(b) that the trend of the experiment Sb *K*-XANES of the InSb QDs has been reproduced quantitatively by the calculated spectrum of InSb QDs embedded in SiO_2 matrix.

To explore the changes that occur in the Sb *K*-XANES of the InSb QDs embedded in SiO_2 matrix well, we have calculated two kinds of Sb *K*-XANES spectra of a six-shell InSb cluster for comparison. One is a naked six-shell InSb cluster, in which both radii of FMS and SCF calculations are 8.0 Å. The other is a six-shell InSb cluster embedded in SiO_2 matrix, in which the cluster radius of FMS calculation is the same as that of the naked six-shell InSb cluster (i.e., 8.0 Å) and the cluster radius of the SCF calculation is 9.1 Å. It needs be mentioned that the cluster with the radius of 9.1 Å is adequate to obtain sufficiently accurate potential of the SiO_2 matrix. Figure 8 demonstrates the calculated spectra for the naked six-shell InSb cluster and the six-shell InSb cluster embedded in SiO_2 matrix, their corresponding atomic background μ_0, and the bulk InSb model with 239 In and Sb atoms (i.e., 135 Sb and 104 In atoms).

V. DISCUSSION

The sharp diffraction peaks in Fig. 5 indicate that the InSb QDs are crystallized quite well, revealing that the growth temperature of 573 K is feasible to form nanocrystalline InSb. Since the preparation conditions of our InSb QDs are similar to those reported by Shi *et al.*,[36] in which their TEM image has shown that the average size of uniform InAs grains grown on Si (111) at 573 K is about 8 nm, we may consider that the grains of InSb QDs with the size of about 30 nm are relatively uniform. Moreover, the XRD pattern of our InSb QDs sample displays that no Sb-oxide (Sb_2O_3 or Sb_2O_5) phase appears.

Table I shows the structural parameters of InSb QDs embedded in SiO_2 matrix. The R,N, and Debye-Waller factor σ^2 of the Sb-In first shell of the InSb QDs are 2.79 Å, 2.8, and 0.00559 Å^2, respectively. The $R_{\text{Sb-In}}$ (2.79 Å) of the InSb QDs is about 0.02 Å smaller than that of the bulk InSb. In addition, Fig. 5 shows that the positions of three XRD diffraction peaks of the InSb QDs shift obviously up to high 2θ direction, indicating that the lattice of the InSb QDs embedded in SiO_2 matrix shrinks slightly with respect to that of the bulk InSb. It is well known that there are mainly two forces affecting the nanocrystals embedded in SiO_2 matrix.[22,30,31,37] One is the thermal expansion force caused by the mismatch of the different thermal expansion coefficient of InSb and SiO_2, and the other is the interface covalent force originated from Sb-O bridge bonds because the binding energy of Sb3*d* is close to that of O1*s*. Therefore, the resultant interaction force on the InSb QDs by the SiO_2 matrix is considered as the compressive strain. The lattice contraction of the InSb QDs obtained from EXAFS and XRD results reveals that the local structure of the InSb QDs has substantially been modified by the SiO_2 matrix due to both the compressive strain on InSb QDs by the SiO_2 matrix and the minimization of InSb QDs surface energy by distorting as well as shrinking. The Debye-Waller factor σ^2 of the Sb-In first shell of the InSb QDs is notably larger than that of the bulk InSb, indicating the presence of the lattice distortion in InSb QDs. Furthermore, the slight left shift and the obvious asymmetry distribution for the anharmonic mean force potential $V(R)$ of the InSb QDs imply that the local structure of InSb QDs is obviously distorted. In contrast, the sharp XRD diffraction peaks without obvious broadening as shown in Fig. 5 display the highly crystalline appearance in InSb QDs, suggesting the preservation of long-range order in the InSb QDs. Therefore, we consider that the enhancement of disorder in InSb QDs is mainly attributed to the structural distortion of interface area. Similarly, these results have reported by Fujii *et al.*,[37] Armelles *et al.*,[22] Ankudinov *et al.*,[38] and Gilbert *et al.*.[39]

Compared with that of bulk InSb, the intensity of the Sb-In first coordination peak of the InSb QDs as shown in Fig. 2(b) remarkably drops by about 25%. Moreover, a small peak corresponding to the Sb-O nearest neighbors appears at about 1.60 Å. We consider that the small peak of Sb-O shell is contributed by the Sb-O bridge bonds between the interface of InSb QDs and SiO_2 matrix, since no Sb oxide phases appear in the XRD pattern and the Sb *K*-XANES spectrum of the InSb QDs. Furthermore, as shown in Table I, the R,N, and Debye-Waller factor σ^2 of the Sb-O nearest neighbors of the InSb QDs are 1.86 Å, 1.0, and 0.00363 Å^2, respectively. The large ratio (about 36%) of Sb-O to Sb-In coordination number in the first shell of the InSb QDs embedded in SiO_2 matrix shows further that there are strong Sb-O bridge bonds between the interface of InSb QDs and the SiO_2 matrix. The Sb-O bond length $R=1.86$ Å reveals unambiguously that the bridge bonds are Sb-O covalent bonds.

Although the average size of the InSb QDs is about 30 nm, which is much bigger than the average size of about 8 nm for the InAs QDs reported by Zhu *et al.*,[23] the RS results indicate that the phonon confinement effect of the InSb QDs is still strong enough. On the other hand, the lattice contraction of the InSb QDs can lead to blue shift of RS spectrum.[22] According to Grüneisen parameter $\gamma=-\partial \ln \omega / \partial \ln V$, one can easily estimate the blueshift of phonon frequencies.[35] The measured Grüneisen parameter for TO mode has the common value of $\gamma=1.41$ for InSb.[40] Our EXAFS and XRD results show that the bond length $R_{\text{Sb-In}}$ of the Sb-In first shell of the InSb QDs contracts by about 0.02 Å, the blueshift of TO phonon frequency should be, therefore, estimated as 3.9 cm^{-1}. Because the total redshift of TO phonon frequency is about 1.1 cm^{-1} as shown in Fig. 1, the redshift of the TO phonon frequency due to the phonon confinement effect of the RS spectrum for the InSb QDs embedded in SiO_2 matrix should actually be about 5.0 cm^{-1}. This result is in good agreement with those reported by Armelles *et al.*[22] and Zhu *et al.*.[23] The phonon confinement effect can be significantly reduced by the accompanying interface effect due to the lattice contraction of InSb QDs.

As seen in Fig. 7, although the two-shell InSb cluster with 17 atoms (i.e., 13 Sb and 4 In atoms) can almost reproduce the features of the Sb *K*-XANES of the bulk InSb, at least five-shell InSb cluster with 47 In and Sb atoms need to be taken into account to simulate the entire fine structures of the Sb *K*-XANES of the bulk InSb. The calculated spectrum of InSb cluster with 167 In and Sb atoms is completely identical with that of InSb cluster with 239 In and Sb atoms. To simulate the possible presence of InSb QDs embedded in SiO_2 matrix, we have considered an average of Sb *K*-XANES for the six-shell InSb cluster surrounded by SiO_2 framework. The results in Fig. 6 indicate that the average Sb *K*-XANES of the six-shell InSb cluster embedded in SiO_2 matrix can excellently reproduce the experimental spectrum of the InSb QDs. To further investigate the contribution of the multiple scattering from the SiO_2 matrix to the changes of the white line peak, we have simulated a six-shell InSb cluster with and without SiO_2 matrix. Seen in Fig. 8, the six-shell InSb cluster (71 atoms) embedded in SiO_2 matrix can give a similar Sb *K*-XANES spectrum to that of a InSb cluster with 239 atoms. The naked six-shell InSb cluster, in contrast, shows almost the same shape of the Sb *K*-XANES spectrum as the bulk InSb. These results suggest that the changes of the white line peak for the InSb QDs embedded in SiO_2 matrix are not caused by the multiplescattering from the SiO_2 embedding matrix. Meanwhile, another striking feature can be noted that the peak corresponding to the white line region of the atomic background $\mu_0(E)$ for the six-shell InSb cluster with SiO_2 matrix is much higher and wider than that of the naked six-shell InSb cluster. The difference between the calculated Sb *K*-XANES for the six-shell InSb cluster with and without SiO_2 matrix is mainly caused by their atomic background absorption $\mu_0(E)$ or the AXAFS.[41–43] This feature exhibits evidently that the change in the white line peak of the Sb *K*-XANES for the InSb QDs embedded in SiO_2 matrix is primarily a local single-site effect on $\mu_0(E)$ due to the effect of SiO_2 matrix on Sb intra-atomic (or embedded atom) potential, and the Sb-O bridge bonds affect indirectly the spectra through the induced changes of the local potential around Sb atoms. Similarly, Ankudinov *et al.* have reported that the $\mu_0(E)$ of Pt NPs is affected by the absorbed hydrogen.[44]

The white line peak of the Sb *K*-XANES of the InSb sample is attributed to the Sb $1s \rightarrow 5p$ dipole transition. The integrated white line intensity of *K*-XANES is commonly associated with the number of the unoccupied n*p* electrons.[45] Since the electronegativity of O atom is notably greater than that of Sb atom, the obvious charge transfer is expected due to the presence of about 26% covalent Sb-O bridge bonding between InSb QDs and SiO_2 matrix. Hence, the change in 5*p*-electron occupation of the Sb atoms should not be negligible. Our XANES calculations from FEFF8 show that the 5*p*-electron occupation of the absorber Sb for the six-shell InSb cluster with and without SiO_2 matrix is about 2.827 e/atom and 3.006 e/atom, respectively. It means that about 0.179 e/atom charge transfers from the 5*p* electron of the absorber Sb to the 2*p* of the O backscattering atom. This result reveals that the intensity increase of the white line peak for the InSb QDs embedded in SiO_2 matrix comes partly from the increase in 5*p*-hole population (*p*-electron depletion of Sb atoms in the InSb QDs), which is in good agreement with the electronegativity consideration. Therefore, the interface effect between the InSb QDs and the SiO_2 matrix can alter the 5*p*-hole population of Sb atom, and enhance the intensity of the white line peak of the Sb *K*-XANES spectrum for the InSb QDs embedded in SiO_2 matrix.

VI. CONCLUSION

In this work the interaction between the InSb QDs and SiO_2 matrix has been investigated by means of RS, XRD, and XAFS. The results of EXAFS and XRD show clearly that the Sb-In bond length of the first shell of the InSb QDs contracts slightly by about 0.02 Å compared with the value in InSb bulk, due to the compressive strain imposed on the InSb QDs by the SiO_2 matrix and the lattice distortion to minimize the surface energy. Furthermore, the lattice contraction partly weakens the phonon confinement effect in RS spectrum. The EXAFS results reveal unambiguously that the bridge bonds between the interface of the InSb QDs and the embedding matrix SiO_2 are mainly Sb (In)-O covalent bonds. The structural disorder in InSb QDs is increased, and the mean force potential $V(R)$ exhibits obvious shape asymmetry. This can be attributed to the strain-induced structural distortion of interface that arises from the competing attempts of the structurally diverse terminating surfaces that encompass the InSb QDs to adopt lower energy configurations. The Sb *K*-XANES simulations of InSb QDs embedded in SiO_2 matrix show that the intensity increase and broadening of the white line peak are mainly due to the increase of Sb *p*-hole occupation and the change of Sb intra-atomic potential affected by the SiO_2 matrix. Therefore, the interaction between the InSb QDs and SiO_2 matrix not only leads to the slight lattice contraction of InSb QDs and obvious structural distortion of interface, but also results in the significant change of the Sb intra-atomic potential and the obvious charge redistribution of Sb atoms.

ACKNOWLEDGMENTS

We would like to thank Professor C. X. Li and A. V. Soldatov for their valuable discussions. This project was supported by the National Science Foundation of China (Grant No. 10375059 and 10174068) and the Knowledge Innovation Program of Chinese Academy of Sciences.

*Electronic address: sqwei@ustc.edu.cn

[1] P. Moriarty, Rep. Prog. Phys. **64**, 297 (2001).

[2] P. Gloria and A. Ramon, Phys. Rep. **395**, 1 (2004).

[3] J. G. Hou, Bing Wang, Jinlong Yang, Kedong Wang, Wei Lu, Zhenyu Li, Haiqian Wang, D. M. Chen, and Qingshi Zhu, Phys. Rev. Lett. **90**, 246803 (2003).

[4] Dana A. Schwartz, Nick S. Norberg, Quyen P. Nguyen, Jason M. Parker, and Daniel R. Gamelin, J. Am. Chem. Soc. **125**, 13205 (2003).

[5] J. S. Steckel, S. Coe-Sullivan, V. Bulovic, and M. G. Bawandi, Adv. Mater. (Weinheim, Ger.) **15**, 1862 (2003).

[6] M. Sugawara, *Semiconductors and Semimetals* (Academic Press, New York, 1999), Vol. 60.

[7] A. V. Uskov, E. P. O'Reilly, R. J. Manning, R. P. Webb, D. Cotter, M. Laemmlin,. N. N. Ledentsov, and D. Bimberg, IEEE Photon. Technol. Lett. **16**, 1265 (2004).

[8] M. T. Todaro, M. De Giorgi, V. Tasco, M. De Vittorio, R. Cingolani, and A. Passaseo, Appl. Phys. Lett. **84**, 2482 (2004).

[9] Y. K. Su, S. J. Chang, L. W. Ji, C. S. Chang, L. W. Wu, W. C. Lai, T. H. Fang, and K. T. Lam, Semicond. Sci. Technol. **19**, 389 (2004).

[10] A. V. Uskov, T. W. Berg, and J. Mork, IEEE J. Quantum Electron. **40**, 306 (2004).

[11] L. W. Ji, Y. K. Su, S. J. Chang, S. H. Liu, C. K. Wang, S. T. Tsai, T. H. Fang, L. W. Wu, and Q. K. Xue, Solid-State Electron. **47**, 1753 (2003).

[12] K. Zhu, Q. Shao, and J. Shi, Chin. Phys. Lett. **18**, 779 (2001).

[13] K. Zhu, J. Shi, and L. Zhang, Solid State Commun. **107**, 79 (1998).

[14] E. Alphandéry, R. J. Nicholas, N. J. Mason,. B. Zhang, P. Möck, and GR Booker, Appl. Phys. Lett. **74**, 2041 (1999).

[15] E. Alphandery, R. J. Nicholas, N. J. Mason, S. G. Lyapin, and P. C. Klipstein, Phys. Rev. B **65**, 115322 (2002).

[16] R. A. Child, R. J. Nicholas, N. J. Mason, P. Shields, J.-P. R. Wells, I. V. Bradley, J. Phillips and B. N. Murdin, Phys. Rev. B **68**, 165307 (2003).

[17] M. L. Steigerwald, and L. E. Brus, Acc. Chem. Res. **23**, 183 (1990).

[18] A. P. Alivisatos, J. Phys. Chem. **100**, 13 226 (1996).

[19] P. Zhang, and T. K. Sham, Phys. Rev. Lett. **90**, 245502 (2003).

[20] H. Zhang, B. Gilbert, F. Huang, and J. F. Banfield, Nature (London) **424**, 1025 (2003).

[21] N. Daldosso, M. Luppi, S. Ossicini, E. Degoli, R. Magri, G. Dalba, P. Fornasini, R. Grisenti, F. Rocca, L. Pavesi, S. Boninelli, F. Priolo, C. Spinella, and F. Iacona, Phys. Rev. B **68**, 085327 (2003).

[22] G. Armelles, T. Utzmeier, P. A. Postigo, and F. Briones, J. Appl. Phys. **81**, 6339 (1997).

[23] K. Zhu, J. Shi, and Q. Shao, Acta Phys. Sin. **49**, 2304 (2000).

[24] Bin Sheng, Dongliang Chen, Jiangwei Fan, Wenhan Liu, Xinfeng Zhang, Yong Jiang, Wensheng Yan, and Shiqiang Wei, Phys. Scr., **T115**, 733 (2005).

[25] Y. Yamamoto, T. Miura, T. Teranishi, M. Miyake, H. Hori, M. Suzuki, N. Kawamura, H. Miyagawa, T. Nakamura, and K. Kobayashi, Phys. Rev. Lett. **93**, 116801 (2004).

[26] A. L. Ankudinov, B. Ravel, J. J. Rehr, and S. D. Conradson, Phys. Rev. B **58**, 7565 (1998).

[27] T. Uruga, H. Tanida, Y. Yoneda, K. Takeshita, S. Emura, M. Takahashi, M. Harada, Y. Nishihata, Y. Kubozono, T. Tanaka, T. Yamamoto, H. Maeda, O. Kamishima, Y. Takabayashi, Y. Nakata, H. Kimura, S. Goto, and T. Ishikawa, J. Synchrotron Radiat. **6**, 143 (1999).

[28] W. J. Zhong and S. Q. Wei, J. Univ. Sci Tech. China **31**, 328 (2001).

[29] E. A. Stern, M. Newville, B. Ravel, D. Haskel, and Y. Yacoby, Physica B **208/209**, 117 (1995).

[30] Shi Jianzhong, Zhu Kaigui, Zheng Qingqi, Zhang Lide, Ye Ling, Wu Jianxin, and Zuo Jian, Appl. Phys. Lett. **70**, 2586 (1997).

[31] H. Richter, Z. P. Wang, and L. Ley, Solid State Commun. **39**, 625 (1981).

[32] G. Dalba, P. Fornasini, R. Grisenti, D. Pasqualini, D. Diop, and F. Monti, Phys. Rev. B **58**, 4793 (1998).

[33] M. Newville, Ph. D. thesis, University of Washington, 1995.

[34] P. Scherrer, Nachr. Ges. Wiss. Göttingen, Math.-phy. Klasse **2**, 98 (1918)

[35] G. Scamarcio, M. Lugara, and D. Manno, Phys. Rev. B **45**, R13 792 (1992).

[36] J. Shi, K. Zhu, W. Yao, and L. Zhang, J. Cryst. Growth **186**, 480 (1998).

[37] M. Fujii, S. Hahashi, and K. Yamanoto, Appl. Phys. Lett. **57**, 2692 (1990).

[38] A. L. Ankudinov, J. J. Rehr, J. J. Low, and S. R. Bare, J. Chem. Phys. **116**, 1911 (2002).

[39] Benjamin Gilbert, Feng Huang, Hengzhong Zhang, Glenn A. Waychunas, and Jillian F. Banfield, Science **305**, 651 (2004).

[40] K. Aoki, E. Anastassakis, and M. Cardona, Phys. Rev. B **30**, 681 (1984).

[41] B. W. Holland, J. B. Pendry, R. F. Pettifer, and J. Bordas, J. Phys. C **11**, 633 (1978).

[42] J. J. Rehr, C. H. Booth, F. Bridges, and S. I. Zabinsky, Phys. Rev. B **49**, R12 347 (1994).

[43] A. Filipponi and A. Di Cicco, Phys. Rev. B **53**, 9466 (1996).

[44] A. L. Ankudinov, J. J. Rehr, J. Low, and S. R. Bare, Phys. Rev. Lett. **86**, 1642 (2001).

[45] *X-ray Absorption: Principles, Applications, Techniques of EXAFS, SESAFS, and XANES*, edited by D. C. Koningsberger and R. Prins (Wiley, New York, 1988).